Structural Analysis of the Neuronal SNARE Protein Syntaxin-1A[†,‡]

Jeffrey C. Lerman,[§] James Robblee,[||] Robert Fairman,[||] and Frederick M. Hughson*[,§]

Department of Molecular Biology, Princeton University, Princeton, New Jersey 08544, and Department of Cell, Molecular, and Developmental Biology, Haverford College, Haverford, Pennsylvania 19041

Received February 21, 2000; Revised Manuscript Received May 11, 2000

ABSTRACT: Intracellular trafficking depends on the docking and fusion of transport vesicles with cellular membranes. Central to docking and fusion is the pairing of SNARE proteins (soluble NSF attachment protein receptors) associated with the vesicle and target membranes (v- and t-SNAREs, respectively). Here, the X-ray structure of an N-terminal conserved domain of the neuronal t-SNARE syntaxin-1A was determined to a resolution of 1.9 Å using multiwavelength anomalous diffraction. This X-ray structure, which is in general agreement with an NMR structure of a similar fragment, provides new insight into the interaction surface between the N-terminal domain and the remainder of the protein. In vitro characterization of the intact cytoplasmic domain of syntaxin revealed that it forms dimers, and probably tetramers, at low micromolar concentrations, with concomitant structural changes that can be detected by limited proteolysis. These observations suggest that the promiscuity characteristic of pairing between v-SNAREs and t-SNAREs extends to the formation of homo-oligomeric t-SNARE complexes as well. They also suggest a potential role for the neuronal Sec1 protein (nSec1) in preventing the formation of syntaxin multimers.

Neurotransmitter release requires three members of the SNARE[1] family of proteins: syntaxin, SNAP-25, and synaptobrevin (also called VAMP). The complex formed by these three proteins is likely to provide an intimate physical link between synaptic vesicles and the plasma membrane at nerve terminals and thereby to facilitate membrane fusion (*1*−*3*). These SNAREs, and especially syntaxin, also interact directly with a number of additional proteins important for synaptic transmission (*4*).

Syntaxin-1A is a 288-residue type II integral membrane protein; residues 1−265 constitute the cytoplasmic domain, while residues 266−288 form the carboxy-terminal transmembrane anchor (*5*). Among the three SNARE proteins required for neurotransmitter release, only syntaxin appears to adopt a well-folded tertiary structure in the absence of the other two SNAREs (*6*, *7*). By contrast, SNAP-25 and the cytoplasmic domain of synaptobrevin are largely disordered under physiological conditions, folding only upon SNARE complex formation.

Like all other SNARE proteins, the juxtamembrane region of syntaxin contains heptad repeats of hydrophobic residues (spanning residues 195−254) consistent with formation of a coiled coil structure (*8*). Indeed, syntaxin forms an SDS-resistant complex with SNAP-25 and synaptobrevin in which this juxtamembrane region contributes one helix to a bundle of four parallel α-helices (*3*). This configuration, which would draw the transmembrane domains of synaptobrevin (anchored in the synaptic vesicle) and syntaxin (anchored in the presynaptic plasma membrane) into close proximity, is likely to facilitate membrane fusion and consequent neurotransmitter release.

In addition to the C-terminal transmembrane anchor and the juxtamembrane region that binds the other SNARE proteins, syntaxin has an approximately 15 kDa N-terminal domain that appears as a flexible arm in electron micrographs of SNARE complexes (*1*). This domain survives limited proteolysis of SNARE complexes (*9*). Despite limited sequence conservation, protease-resistant N-terminal domains are a very common feature among widely diverse syntaxin family members (*10*; L. Cavanaugh and F. M. Hughson, unpublished). Two potential roles, which are not mutually exclusive, have been ascribed to these N-terminal domains. Studies with syntaxin and with its yeast homologue Sso1p have suggested that the N-terminal domain inhibits SNARE assembly, presumably by binding intramolecularly to the juxtamembrane domain to produce a "closed" conformation (*7*, *11*−*13*). A second potential role is in binding to other proteins with important roles in neurotransmitter release; the binding site of Munc13 has been localized within the N-terminal domain of syntaxin (*14*), and binding of the

[†] This work was supported by NIH Grant NS-38046, the Searle Scholars Program, and the Beckman Young Investigators Program (F.M.H.).

[‡] X-ray coordinates and structure factors have been deposited in the Research Collaboratory for Structural Bioinformatics, Rutgers University, New Brunswick, NJ (1EZ3).

* To whom correspondence should be addressed. Telephone: (609) 258-4982. Fax: (609) 258-6730. E-mail: hughson@princeton.edu.

[§] Princeton University.

[||] Haverford College.

[1] Abbreviations: CD, circular dichroism; DTT, dithiothreitol; HEPES, 4-(2-hydroxyethyl)piperazine-1-ethanesulfonic acid; MAD, multiwavelength anomalous diffraction; nSec1, neuronal Sec1 protein; NSF, *N*-ethylmaleimide-sensitive fusion protein; PAGE, polyacrylamide gel electrophoresis; PEG, polyethylene glycol; SDS, sodium dodecyl sulfate; SeMet, selenomethionine; SNAP-25, synapse-associated protein (25 kDa); SNARE, soluble NSF attachment protein receptor; t-SNARE, target membrane SNARE; v-SNARE, vesicle SNARE; SRV, square root of variance; VAMP, vesicle-associated membrane protein.

10.1021/bi0003994 CCC: $19.00 © 2000 American Chemical Society
Published on Web 06/23/2000

neuronal Sec1 protein (nSec1; also called Munc18) is dependent on this domain as well as on the juxtamembrane region (*15*). nSec1 binds to a closed syntaxin conformation (*16*), and mutations that apparently destabilize this closed conformation compromise binding (*7*).

Fernandez et al. (*17*) have used solution NMR to characterize the structure of the N-terminal domain of syntaxin-1A. They found that residues 1−180, expressed as a recombinant protein in *Escherichia coli*, contained disordered ends, but that residues 27−146 formed an independently folded domain. Structural analysis, using residues 27−146 with Cys 146 replaced with Ser, revealed a three-helix bundle with a left-handed twist (*17*). The groove between the second and third helices is formed by residues that are highly conserved among plasma membrane syntaxins (*17*).

Here, we describe biophysical studies that provide further insight into the overall structural organization of syntaxin-1A. In particular, the X-ray structure of residues 24−150 has been determined and refined to 1.9 Å resolution. While this structure is similar to that previously determined by NMR spectroscopy (*17*), there are a number of differences, particularly for residues that define the interactive surface of the molecule. The X-ray structure reveals that the groove between the second and third helices is not only conserved but also quite hydrophobic, strengthening the hypothesis that, in the closed form of intact syntaxin, it is involved in interactions with the juxtamembrane region. Furthermore, we have characterized the oligomeric state of the intact cytoplasmic domain (residues 1−265) of syntaxin and find that dimeric and probably tetrameric forms are significantly populated at low micromolar protein concentrations. Syntaxin dimers and tetramers may result from the parallel alignment of juxtamembrane regions into a helical bundle structure resembling that of the SNARE complex. These results add a new level of complexity to previous findings suggesting that heteromeric SNARE complex formation can be promiscuous (*10*, *18*, *19*), demonstrating that SNAREs can self-partner as well.

EXPERIMENTAL PROCEDURES

Materials. All chemicals used for crystallization were purchased from Fluka. Other materials were purchased from Sigma (subtilisin, amino acids, and trace metal salts), Boehringer Mannheim (proteinase K), and Novagen (BL21 & B834 *E. coli* strains).

Protein Expression. Protein expression plasmids were constructed in pLM1 (*20*), a T7 promoter plasmid, using PCR. The correctness of the coding sequence was confirmed by DNA sequencing. Protein was expressed in *E. coli* BL21(DE3) cells, except that BL21(DE3)(pLysS) cells were used for production of syntaxin 1−265 and B834(DE3) cells were used for the selenomethionine (SeMet) derivative of syntaxin 24−150.

SeMet Derivative Expression. SeMet-substituted syntaxin 24−150 was expressed essentially as described previously (*21*) in modified M9 medium except that the starter culture was supplemented with 5% LB medium and several amino acids (alanine, aspartate, glutamate, glycine, histidine, asparagine, proline, glutamine, serine, tryptophan, and tyrosine) were omitted from the modified M9 medium. SeMet incorporation was confirmed by mass spectrometry.

Protein Purification. Syntaxin 24−150 (both the native form and the SeMet derivative) was purified using Q-Sepharose and phenyl-Sepharose columns and exchanged into 10 mM dithiothreitol (DTT) by repeated concentration and dilution in a centrifuge concentrator (Millipore). Syntaxin 1−253 and syntaxin 1−265 were purified by recovery from inclusion bodies as described previously (*22*), subsequent refolding by rapid dilution, and concentration by binding to a Q-Sepharose column. The identity of the purified proteins was confirmed by mass spectrometry.

Crystallization. Native syntaxin 24−150 was crystallized by the hanging drop method. One microliter of 4 mg/mL protein in 10 mM DTT was added to 1 μL of reservoir solution [16% polyethylene glycol (PEG) 1500, 20 mM sodium acetate (pH 5.0), and 10 mM DTT] on a coverslide which was inverted over 1 mL of reservoir solution. Crystals grew over a period of 1−4 days at 23 °C. SeMet syntaxin 24−150 derivative crystals grew under the same conditions, except that the protein stock contained 8 mg/mL protein, 20 mM DTT, and 30 mM sodium acetate (pH 5.0).

X-ray Data Collection. Crystals were equilibrated in several steps over 10 h into reservoir solution supplemented with 18% glycerol and flash-frozen in a 100 K nitrogen cold stream (Oxford). Data were collected at beamline X12C at the National Synchrotron Light Source at Brookhaven National Labs.

X-ray Data Processing. Data were indexed and scaled using Denzo and Scalepack from the HKL software package (version 1.11.0) (*23*). Initial phases were calculated from a multiwavelength anomalous diffraction (MAD) data set using MLPHARE and DM (*24*) and were later extended with higher-resolution native data using X-PLOR (*25*) and CNS version 0.5 (*26*). Cycles of model building and refinement were carried out using X-PLOR, CNS, and O (*27*).

Protease Digestion. Syntaxin was exchanged into digestion buffer [150 mM NaCl, 5 mM HEPES (pH 7.4), and 1 mM DTT] using NAP-5 columns (Pharmacia), diluted to the working concentration using additional digestion buffer, and incubated on ice for 2 h to allow equilibration among oligomeric states. Subtilisin was added to a substrate:protease weight ratio of 90:1 to start the reaction. At the indicated time points, samples were taken from the reaction and the reactions stopped with 1 mM phenylmethanesulfonyl fluoride followed by freezing in liquid nitrogen. After samples at all time points had been collected, they were thawed, concentrated by trichloroacetic acid precipitation (15%), and analyzed by SDS−PAGE. In separate experiments, several of the digestion products were partially purified and characterized by amino-terminal sequencing and mass spectrometry.

Circular Dichroism. Circular dichroism (CD) data were collected using an AVIV 62DS CD spectrometer and a sample containing 10 μM syntaxin 24−150 in 1 mM β-mercaptoethanol, 100 mM KF, and 1 mM sodium phosphate (pH 7.5). Spectra from three consecutive scans (250−190 nm, 1 s averaging time, and 0.25 nm steps) were averaged. For thermal unfolding experiments, data at 222 nm were recorded (1 min temperature equilibration, 0.5 min averaging time, and 1 °C steps).

Analytical Ultracentrifugation. Protein was exchanged into digest buffer containing 0.5 mM DTT. Sedimentation equilibrium experiments were performed at 4 °C with a Beckman Optima XL-A analytical ultracentrifuge at rotor speeds of

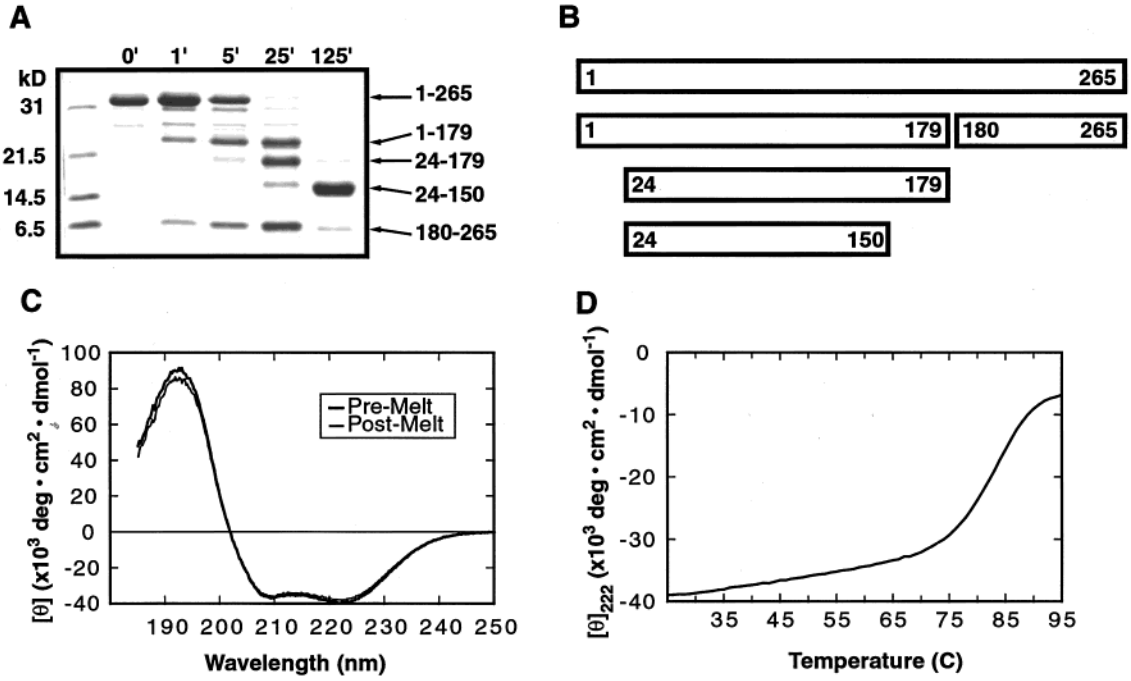

FIGURE 1: Subtilisin digestion of the syntaxin cytoplasmic domain yields a protected N-terminal structural domain. (A) Recombinant syntaxin 1−265 (2 μM) was mixed with subtilisin (90:1 w/w) on ice. Samples were withdrawn at the indicated times after protease addition, and phenylmethanesulfonyl fluoride was added to a concentration of 1 mM to quench the reaction. Samples were analyzed on Coomassie-stained SDS−PAGE gels. Digestion products as indicated were identified by amino-terminal sequencing and mass spectroscopy. (B) Schematic interpretation of panel A. The initial products of digestion are fragments 1−179 and 180−265. Fragment 1−179 is subsequently trimmed to 24−179 and ultimately to 24−150. (C) The CD spectrum of syntaxin 24−150 at 25 °C (black trace) indicates >90% α-helix content. Almost complete reversibility is observed after heating to 95 °C and subsequent cooling back to 25 °C (gray trace). (D) Syntaxin 24−150 unfolds cooperatively with temperature as judged by its mean residue ellipticity at 222 nm.

8000, 12 000, 16 000, and 20 000 rpm using an An-60 Ti rotor. Six-channel, 12 mm path length, charcoal-filled Epon cells with quartz windows were used. Twenty scans were averaged. Temperature-corrected partial specific volumes of both syntaxin-1A fragments were calculated from the weighted average of the partial specific volumes of the individual amino acids (*28*). Temperature-corrected solution densities were calculated using standard tables listing coefficients for the power series approximation of density (*28*). The HID program from the Analytical Ultracentrifugation Facility at the University of Connecticut (Storrs, CT) was used for data analysis. Equilibrium sedimentation analysis software implemented under IGOR Pro version 3.16 (WaveMetrics Inc., Lake Oswego, OR) using the Marquardt−Levenberg algorithm for curve fitting was used for the preparation of Figure 4.

RESULTS

Syntaxin 24−150. The structure of the cytoplasmic domain of syntaxin-1A (residues 1−265) was probed by limited digestion with nonspecific proteases. Subtilisin (Figure 1A) and proteinase K reactions (data not shown) yielded very similar patterns. In both cases, syntaxin is cleaved first between residues 179 and 180 to yield two fragments, residues 1−179 and 180−265 (Figure 1B). Additional digestion yields a stable product comprising syntaxin residues 24−150. These findings are in good agreement with NMR studies of syntaxin 1−180 indicating that residues 27−146 form a folded domain (*17*). Furthermore, in ternary syntaxin−SNAP-25−synaptobrevin complexes, a similar or identical syntaxin domain is protected from proteolysis by a variety of proteases (*9*).

Syntaxin 24−150, as expected, is highly α-helical (Figure 1C). In addition, it is thermostable, unfolding in a single reversible cooperative transition with a midpoint of approximately 85 °C (Figure 1D). We have determined the X-ray structure of this domain using selenomethionine-substituted syntaxin 24−150. Phases estimated by MAD yielded an electron density map that was, in general, readily interpretable (Figure 2A). The structure was subsequently refined to 1.9 Å resolution (Figure 2B) using data collected from a native crystal (Table 1).

The X-ray structure shows a bundle of three α-helices connected by short loops (Figure 2C,D), as expected on the basis of the NMR structure of syntaxin 27−146 with the point mutation Cys 146 → Ser (*17*). In keeping with the notation introduced there (*17*), the three helices are termed Ha (residues 28−64), Hb (residues 68−105), and Hc (residues 110−146), although each helix is several residues shorter in the NMR structure. The root-mean-square deviation between the NMR and X-ray structures is relatively large (2.1 Å over 124 equivalent C_α atoms). Comparative analysis of the X-ray and NMR structures reveals four principal differences. First, the course of the backbone is well-defined in the X-ray structure for most of the regions that are poorly defined by the NMR structure. Second, many surface side chains are also well-defined in the X-ray, but not the NMR, structure. Third, a few well-defined side chains in the NMR structure occupy significantly different rotamer positions in the X-ray structure (see below). Fourth, the pronounced curvature of the helix bundle observed in the NMR structure

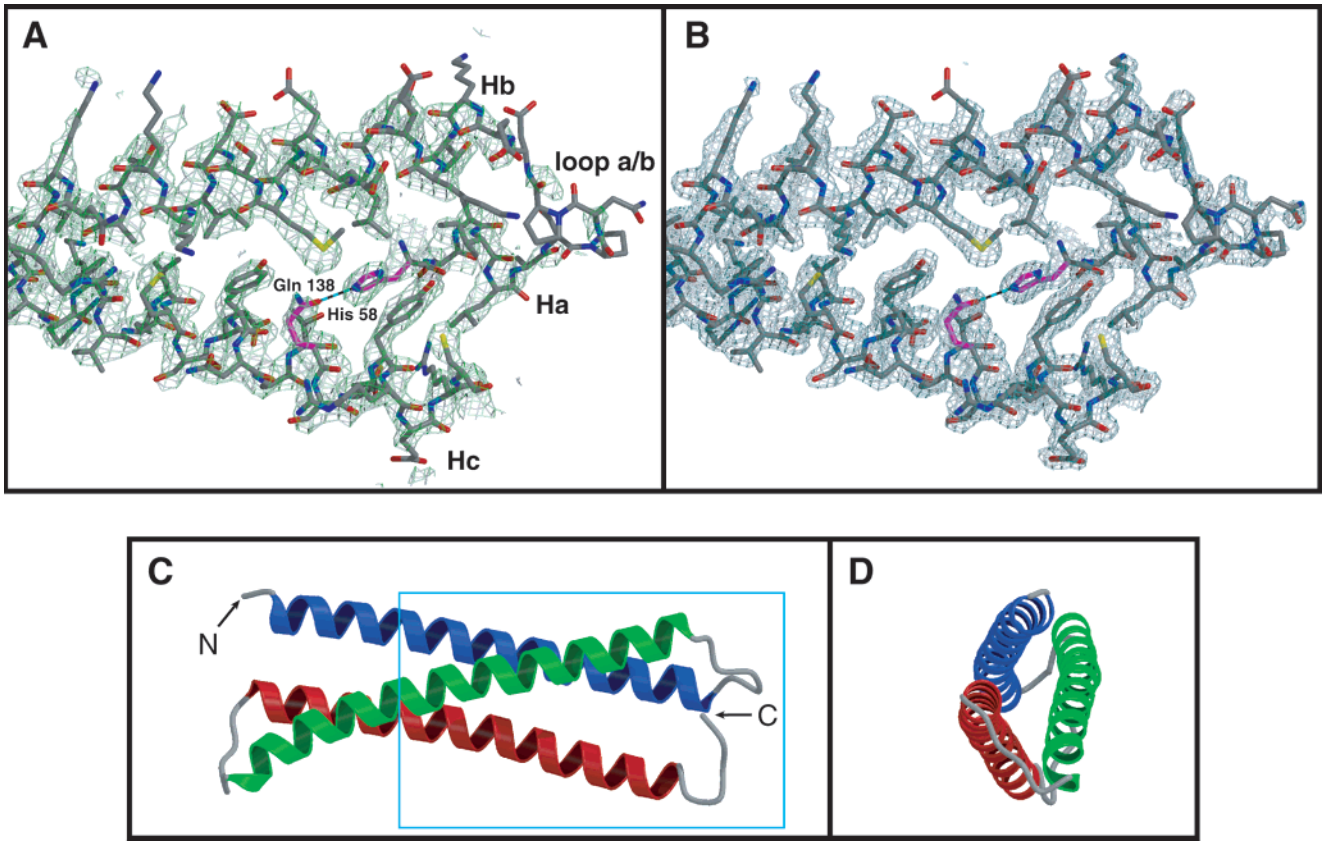

FIGURE 2: Syntaxin 24−150 X-ray structure. (A) A portion of the model corresponding to the box in panel C is shown together with the corresponding regions of the experimental 2.4 Å MAD electron density map contoured at 1.2 σ. Most of helix Ha (residues 27−57) and residues 146−150 are omitted for clarity. The hydrogen-bonded side chains of His 58 and Gln 138 are shown in magenta. (B) σ_A-weighted $2F_o - F_c$ map at 1.9 Å is shown together with the same portion of the model as in panel A. (C) Schematic overview of the structure. Residues 27−150 are shown; residues 24−26 did not appear in the electron density and were not modeled. The structure is built primarily of three α-helices: Ha (residues 28−63; blue), Hb (residues 69−106; green), and Hc (residues 111−145; red). Loop regions are shown in gray. (D) Longitudinal view, where the model is rotated 90° from the orientation shown in panel C, with the N-terminus now toward the viewer. These figures were created using Bobscript (*46*), Molscript (*47*), and Raster3D (*48*).

is not seen in the X-ray structure, in which the bundle is essentially straight. This difference may be attributable to crystal lattice effects or to the lack of long-range distance constraints in the determination of the NMR structure (*29*).

As noted previously (*17*), one side of syntaxin 24−150 is decidedly acidic (Figure 3B). Two patches at either end of the molecule are especially notable. One patch is formed by Asp 68, Glu 69, Glu 73, Glu 74, Glu 76, Glu 77, and Asp 81. Many of these residues participate directly in an interaction between syntaxin and the Ca^{2+}-binding protein syntaptotagmin, thought to be a principal Ca^{2+} sensor in regulating neurotransmitter release (*17*). A second, smaller patch is formed by Glu 32, Glu 35, and Glu 38 (Figure 3B).

A Conserved Hydrophobic Groove. Between helices Hb and Hc is a wide groove (Figure 3A). This groove has a pronounced hydrophobic character resulting from fully (Val 128) or partially (Ile 61, Leu 75, Leu 93, Phe 127, and Met 131) solvent-accessible nonpolar side chains. In the X-ray (but not the NMR) structure, Gln 138 is tucked into the core of the three-helix bundle, hydrogen bonded with the buried side chain of His 58, further increasing the hydrophobic character of the groove (Figure 2A,B). All of these residues are highly conserved among syntaxins implicated in exocytosis. Indeed, the residues lining the Hb−Hc groove are significantly more conserved than those in either of the other two helix−helix interfaces (*17*). The other two interhelical grooves (Figure 3) are less hydrophobic, narrower, and partially occluded by interhelical salt bridges: Lys 57 forms an ion pair with Glu 74, bridging Ha and Hb, while nearby Lys 55 forms a salt bridge network with Glu 52 and Glu 133, bridging Ha and Hc.

Although the exact role of the N-terminal domain in syntaxin function is not known, interactions between the N-terminal domain and the juxtamembrane C-terminal region likely play important roles in regulating SNARE function. Both syntaxin and its yeast homologue Sso1p exist in an equilibrium between closed and open forms, distinguished by whether the N-terminal domain is folded together with the juxtamembrane region (closed) or not (open) (*7*, *12*). In the absence of direct high-resolution information characterizing the closed conformation, two structural models have been proposed in which the three-helix bundle is extended by residues of the juxtamembrane domain to form either a four-helix (*13*) or five-helix (*7*) bundle. In either case, these juxtamembrane regions likely form one or more additional α-helices that pack into the conserved hydrophobic groove observed in the X-ray structure of syntaxin 24−150.

Our initial analysis of syntaxin 1−265, however, provided little evidence for such a closed conformation. The earliest protected proteolytic fragments comprised residues 1−179 and residues 180−265 (Figure 1A,B), and we first suspected that this protection might be afforded by interactions between

Table 1: Data Collection, Phasing, and Refinement Statistics

	Diffraction Data			
	native	Se-edge	Se-peak	Se-remote
wavelength (Å)	0.98	0.9790	0.9785	0.950
maximum resolution (Å)	1.90	2.20	2.20	2.20
no. of unique reflections	29756	19358	19472	18895
no. of total reflections	155471	96366	96132	96310
completeness (%) (last shell[a])	99.9 (99.7)	98.0 (95.1)	98.0 (94.7)	98.2 (96.4)
R_{symm} (%) (last shell)[b]	4.3 (16.3)	8.0 (34.9)	8.9 (35.3)	7.9 (38.9)
I/σ (last shell)	45.5 (9.4)	18.6 (3.0)	20.0 (2.9)	19.5 (2.8)

	Phasing		
	Se-edge	Se-peak	Se-remote
no. of sites	9	9	9
no. of reflections (acentric/centric)	18726/626	18703/620	18221/661
R_{cullis} (acentric/centric)[c]	n/a	0.88/0.85	0.77/0.68
phasing power (acentric/centric)[d]	n/a	0.74/0.55	1.26/1.04
R_{cullis} anomalous (no. of reflections)	0.81 (18603)	0.75 (18582)	0.80 (18162)
overall figure of merit	0.75		

Refinement	
	native
resolution (Å)	8.0−1.90
R_{cryst}/R_{free} (%)[e]	23.1/28.6
no. of atoms (protein/water)	3070/422
mean B factors (Å^2) (protein/water)	36.1/44.9
rmsds	
bond lengths (Å)	0.006
bond angles (deg)	0.97

[a] Last shell of 10 shells; 1.97−1.90 Å for the native data set, and 2.28−2.20 Å for the SeMet data set. [b] $R_{symm} = \Sigma|(I_h - \langle I_h\rangle)|/\Sigma I_h$ over all h, where I_h is the intensity of reflection h. [c] $R_{cullis} = \Sigma||F_{ph} \pm F_p| - |F_h||/\Sigma|F_{ph} \pm F_p|$, where F_{ph} and F_p are the derivative and native structure factors, respectively, and F_h is the calculated heavy-atom structure factor. [d] Phasing power $= \langle F_h\rangle/E$, where $\langle F_h\rangle$ is the root-mean-square heavy-atom structure factor and E is the residual lack of closure error. [e] R_{cryst} and $R_{free} = \Sigma||F_o| - |F_c||/\Sigma|F_o|$. R_{free} was calculated using 5% of the data excluded from refinement.

these fragments. However, they did not comigrate on gel filtration columns, as might have been expected were they associated (data not shown). Furthermore, syntaxin 180−265 exhibited a strong tendency to aggregate, and precipitated from digestion reaction mixtures in which this fragment was present at concentrations of 40−100 μM (data not shown). Thus, the protection of syntaxin 180−265 against proteolytic digestion is not due to association with the N-terminal domain but may instead be attributable to self-association. The finding that syntaxin 180−265 is prone to intermolecular association prompted us to investigate the oligomeric state of syntaxin and whether oligomerization might affect its conformation.

Syntaxin Multimerization. Preliminary gel filtration experiments (not shown) suggested that syntaxin 1−265 formed several self-associated species. To characterize further the nature and energetics of oligomeric syntaxin states, we used analytical equilibrium ultracentrifugation. In addition to syntaxin 1−265, we also analyzed syntaxin 1−253, a product of botulinum neurotoxin C cleavage (*30*) that previous work had suggested might be less susceptible to aggregation (*7*, *17*). Data were collected at four rotor speeds (8000−20000 rpm) and four protein loading concentrations (2−100 μM) to evaluate various self-association models.

We focus first on a discussion of the results for syntaxin 1−253 as this fragment exhibited more limited self-association behavior than did syntaxin 1−265. For syntaxin 1−253, self-association is evident from single-species analysis in which the molecular mass is treated as a fitting parameter. A diagnostic feature for multiple states in solution is that the apparent molecular mass decreases as a function of increasing rotor speed (Table 2). The fact that the additional states are a consequence of self-association follows from the observation that the apparent molecular mass increases from 40 800 ± 3000 Da to 60 900 ± 3400 Da over the range of 2−100 μM (data not shown); the monomer molecular mass is 29 307 Da. Similar results are obtained for syntaxin 1−265, with the apparent molecular mass increasing from 64 300 ± 4900 to 83 400 ± 8300 over this same concentration range (monomer molecular mass of 30 751 Da). These data, in agreement with gel filtration results (not shown) and previous NMR studies (*7*), indicate that syntaxin 1−265 is more prone to oligomerization than syntaxin 1−253.

The single-species analyses prompted us to evaluate a series of models for the oligomeric state(s) of syntaxin 1−253. The square root of variance (SRV) was monitored as a probe of the quality of the fits of various models to the data (Table 2), with a lower SRV indicating a better model. At high rotor speeds, we find that the minimal model which fits the data is a monomer−dimer (1 ↔ 2) model (Table 2). The equilibrium dissociation constant, K_{21}, for this reaction is 9.9 ± 4.6 μM, predicting the formation of a stable dimer. However, it is obvious that this model is insufficient to describe the data at lower rotor speeds. The SRVs for this model are poorer at lower speeds and seem to favor a higher-order, 1 ↔ 3 model. While this observation may, at first, seem inconsistent, it is possible to reconcile the failure of a two-state model analysis by considering a more complex three-state model which includes the 1 ↔ 2 model with the addition of a higher-order oligomeric state. The trend, a decreasing order of the single self-associated state as a function of increasing speed, helps to support this conclusion.

Among the three-state models that were considered, a 1 ↔ 3 ↔ 6 model can be ruled out as this model is no better than the simpler 1 ↔ 3 model and is significantly worse than the two-state 1 ↔ 2 model, as judged by the SRVs reported at 20 000 rpm. In contrast, the SRVs for either a 1 ↔ 2 ↔ 3 or a 1 ↔ 2 ↔ 4 model, in general, are lower than that of any two-state model. While we could not rule out the 1 ↔ 2 ↔ 3 model on the basis of the SRVs alone, this model is less likely because it predicts no significant amount of dimer and, thus, is in disagreement with the amount of dimer that is predicted from the reasonable fit of the 1 ↔ 2 model to the higher-speed data. In contrast, the 1 ↔ 2 ↔ 4 model predicts amounts of dimer similar to that with the 1 ↔ 2 model. Therefore, we favor the 1 ↔ 2 ↔ 4 model.

An identical model analysis of syntaxin 1−265 yields similar results, although in this case it is not possible to distinguish with confidence among the three-state models that are considered. Since this fragment self-associates to a higher degree, we suspect that even more complex models

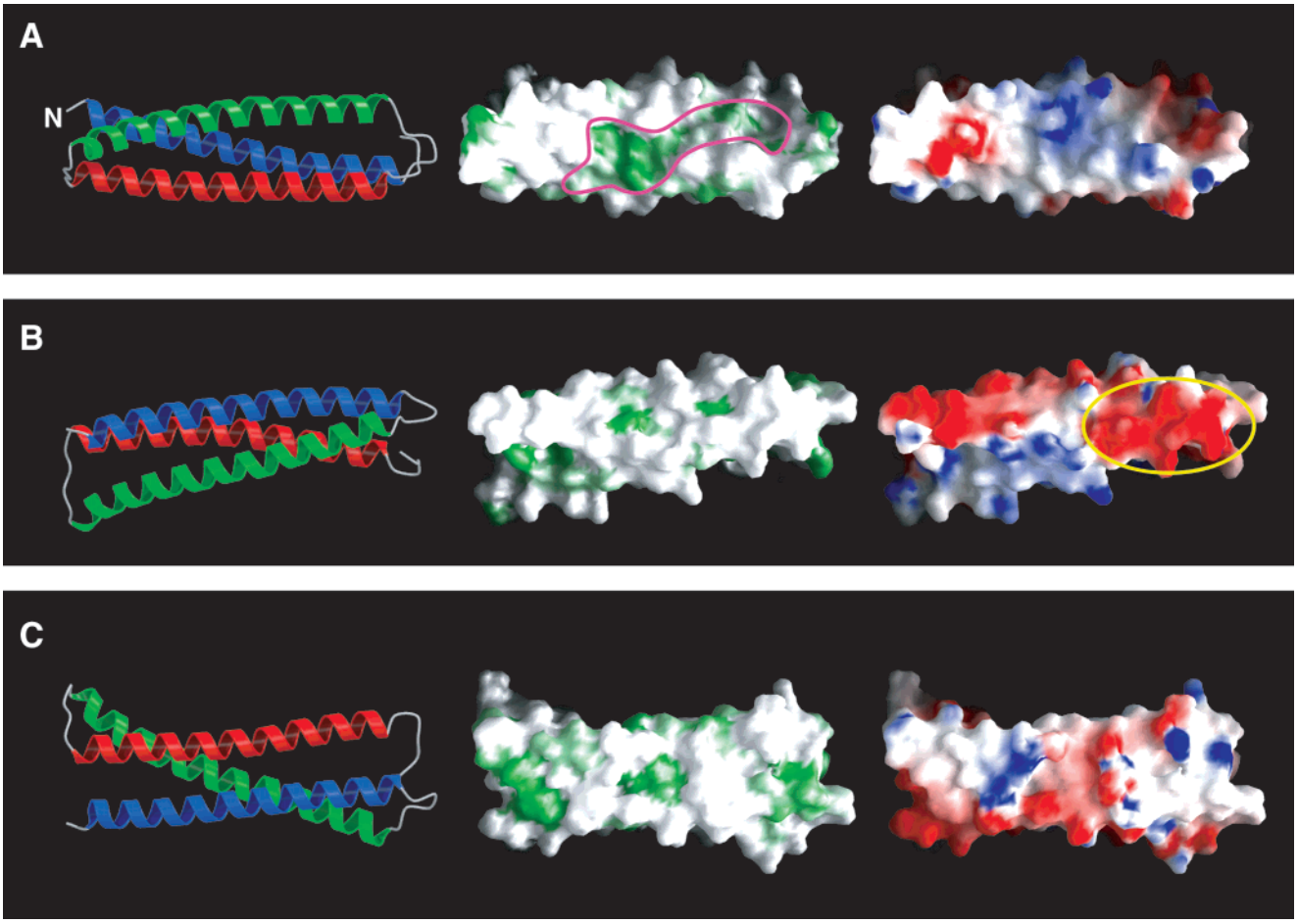

FIGURE 3: Syntaxin 24−150 surface properties. Each panel is organized with a ribbon diagram on the left, a molecular surface coded by hydrophobicity in the center (green is hydrophobic and white is hydrophilic), and a molecular surface coded by electrostatic surface potential on the right (red is acidic and blue is basic). Syntaxin 24−150 has been rotated 120° about its long axis between each successive panel. The groove between helices Hb and Hc, proposed to bind the juxtamembrane helix of syntaxin, is outlined in magenta in panel A. The acidic patch on helices Hb and Hc implicated in binding to synaptotagmin (see the text) is circled in yellow in panel B. These figures were created using Molscript (*47*), Raster3D (*48*), and GRASP (*49*).

Table 2: Sedimentation Equilibrium Ultracentrifugation Data Analyzed as a Function of Speed[a]

	square root of variance ($\times 10^3$)							
	syntaxin 1−253				syntaxin 1−265			
model	8000 rpm	12 000 rpm	16 000 rpm	20 000 rpm	8000 rpm	12 000 rpm	16 000 rpm	20 000 rpm
M_r[b]	82 500 ± 10 400	70 000 ± 4800	57 300 ± 3300	46 300 ± 2800	112 500 ± 14 400	91 700 ± 7100	78 600 ± 4500	64 600 ± 4800
1 ↔ 2	*c*	*c*	5.18	4.95	*c*	*c*	*c*	*c*
1 ↔ 3	4.40	5.89	9.05	10.9	6.17	6.03	5.21	6.94
1 ↔ 4	4.58	9.98	14.2	14.5	5.32	6.10	10.7	12.8
1 ↔ 5	4.98	11.1	15.3	15.3	5.39	9.18	15.9	17.9
1 ↔ 2 ↔ 3	4.40	4.92	4.58	4.95	6.17	6.08	5.19	6.13
1 ↔ 2 ↔ 4	4.40	5.31	4.74	5.00	5.33	5.52	6.44	7.35
1 ↔ 3 ↔ 6	4.40	5.89	9.06	10.9	5.09	5.66	5.21	7.21

[a] The 2, 8, 32, and 100 μM data were analyzed simultaneously at each rotor speed. [b] Molecular mass in daltons, M_r, is calculated from a single-species analysis. [c] The apparent molecular mass was greater than the dimer molecular mass; thus, the model could not be fit to the data.

are required, including states larger than a tetramer. Clear evidence for higher-order aggregation is apparent in an analysis of syntaxin 1−265 at the highest loading concentration (100 μM; data not shown). However, because it differs from syntaxin 1−253 only in the presence of 12 additional C-terminal residues, we hypothesize that syntaxin 1−265 forms stable dimers and tetramers in addition to higher-order oligomers.

We can use these simple models to make predictions about the stabilities of dimers and higher-order oligomeric states. As an example, we assume a 1 ↔ 2 ↔ 4 model based on our analysis of syntaxin 1−253. Equilibrium dissociation constants derived for this model as fit simultaneously to all the data (four rotor speeds and at least three protein loading concentrations) indicate that syntaxin 1−265 dimers (K_{21} = 1.4 ± 0.5 μM) are more stable than syntaxin 1−253 dimers (K_{21} = 5.8 ± 1.8 μM). Strikingly, syntaxin 1−265 tetramers (K_{42} = 12 ± 6 μM) are much more stable than syntaxin 1−253 tetramers (K_{42} = 1.2 ± 0.5 mM). In Figure 4, we show the quality of the fits using this model to the 2 μM

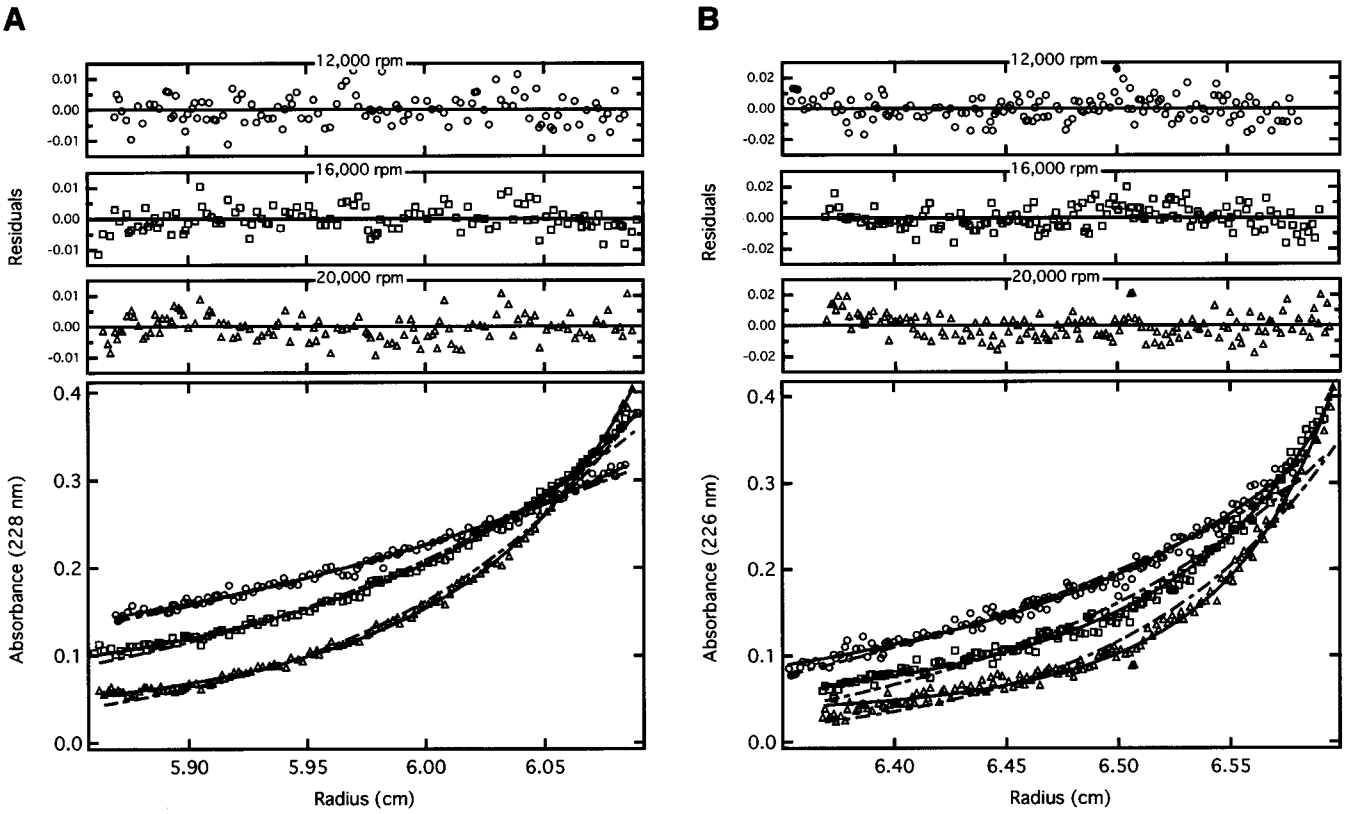

FIGURE 4: Syntaxin forms dimers and higher-order multimers at low micromolar concentrations. (A and B) Sedimentation equilibrium data and fits derived from a 1 ↔ 2 ↔ 4 model. The 2 μM data for syntaxin 1−253 (A) or 1−265 (B) were fit (*50*) using dissociation constants reported in the text. For comparison, we show fits assuming pure monomer (dashed lines). Nonrandom deviations in the fits are evident in this model. If these data alone are fit to a 1 ↔ 2 equilibrium, the fits are indistinguishable from the more complex 1 ↔ 2 ↔ 4 equilibrium scheme.

ultracentrifugation data for both fragments (Figure 4A,B). Although the equilibrium constants reported here are model-dependent, it is clear that at low concentrations both syntaxin fragments dimerize and that syntaxin 1−265 is significantly more prone to self-association.

Self-Association Causes a Conformational Change. The evidence presented so far shows that (i) syntaxin 180−265 aggregates, (ii) syntaxin 1−253 forms dimers and also larger multimers, probably trimers and/or tetramers, and (iii) syntaxin 1−265 self-associates to an even greater extent than syntaxin 1−253. It therefore appears that, in addition to mediating heteromeric interactions with SNAP-25 and synaptobrevin, juxtamembrane regions of syntaxin mediate homomeric interactions. Accordingly, we asked whether conformational changes were associated with homomeric interactions as they are with heteromeric ones (*6*, *12*, *13*, *31*, *32*), using limited proteolysis as a conformational probe. Detailed studies were carried out comparing the limited protease digestion patterns of syntaxin 1−265 and syntaxin 1−253 (Figure 5). A number of the resulting protein fragments were identified by N-terminal sequencing and mass spectrometry.

Initial experiments comparing syntaxin 1−253 and syntaxin 1−265 were carried out at a substrate concentration of 2 μM (Figure 5, central panels). At this concentration, the majority of syntaxin 1−253 is monomeric, whereas the majority of syntaxin 1−265 is dimeric. Surprisingly, syntaxin 1−253 is less susceptible to subtilisin cleavage than syntaxin 1−265, as judged by the disappearance of the full-length protein (A1 or A2 in the central panels of Figure 5). If the native conformation were simply destabilized by truncation, an increase in protease sensitivity for syntaxin 1−253 would have been anticipated. The greater protease sensitivity of syntaxin 1−265 is due to an increased level of cleavage between residues 179 and 180, since the products of this cleavage reaction (C and F2) accumulate rapidly. The accumulation of C is somewhat attenuated by its further digestion to D and E. Taken together, however, the accumulation of C plus D and E is substantially more rapid for syntaxin 1−265 than for syntaxin 1−253. Thus, syntaxin 1−265 is more sensitive to cleavage between residues 179 and 180 than syntaxin 1−253. Furthermore, whereas syntaxin 1−265 is cleaved preferentially between residues 179 and 180, the initial cleavage site for subtilisin on syntaxin 1−253 is between residues 220 and 221. Cleavage at this latter site yields fragment B (residues 1−220) in Figure 5; the corresponding C-terminal fragment is unlikely to be stable, and in any case is too small to visualize using this gel system. This fragment probably corresponds to the structured region of the closed conformation (see the Discussion).

On the basis of these results, we hypothesized that the increased protease sensitivity of syntaxin 1−265 between residues 179 and 180 was coupled to its greater tendency to self-associate (Figure 4). Furthermore, we reasoned that the decreased sensitivity of syntaxin 1−253 at the same site might be attributable to the closed conformation of the monomeric protein. This model is depicted schematically in Figure 6 (see also the Discussion), in which parentheses indicate that a site is inaccessible (or less accessible) to proteolytic cleavage. To further examine the potential

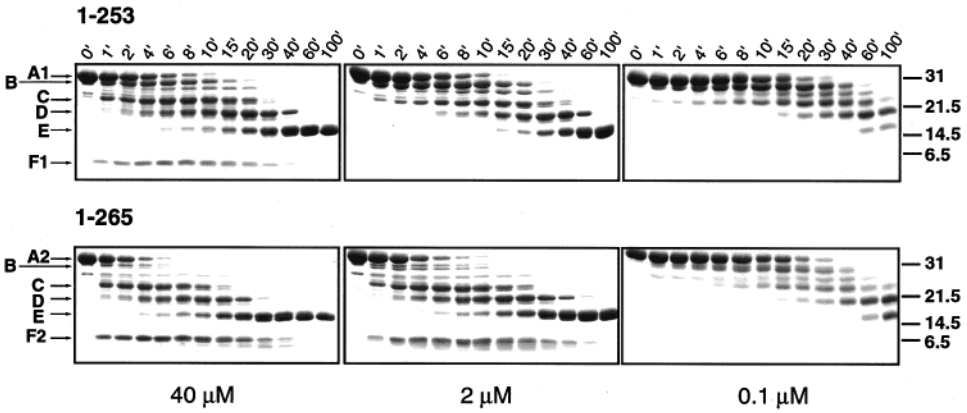

FIGURE 5: Multimerization causes a conformational change in syntaxin. Recombinant syntaxin 1−253 (top) or syntaxin 1−265 (bottom) was subjected to limited subtilisin digestion and analyzed as described in the legend of Figure 1. The initial syntaxin:subtilisin ratio was held constant in all experiments, but three different initial substrate concentrations were tested: 40 μM (left), 2.0 μM (center), and 0.1 μM (right). Molecular masses in kilodaltons are indicated at the far right. Syntaxin digestion products as labeled on the far left were identified by amino-terminal sequencing and mass spectrometry as follows: (A1) 1−253, (A2) 1−265, (B) 1−220, (C) 1−179, (D) 24−179, (E) 24−150, (F1) 180−253, and (F2) 180−265.

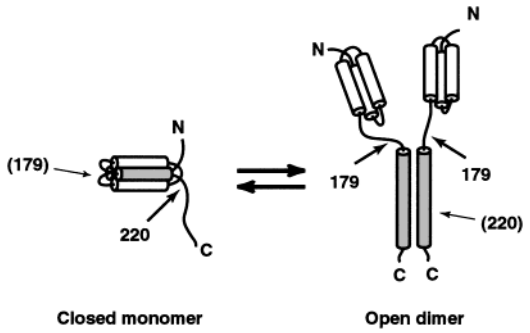

FIGURE 6: Model for syntaxin dimerization mediated by the juxtamembrane region. Closed monomers, represented schematically as four-helix bundles, are preferentially cleaved by subtilisin between residues 220 and 221, while open dimers are preferentially cleaved between residues 179 and 180. Cleavage between residues 179 and 180 is suppressed in monomers by unknown structural features. Little if any cleavage between residues 220 and 221 is observed in multimers; instead, syntaxin 180−265 resulting from initial cleavage is strongly protected from further digestion, as it is in syntaxin−SNAP-25−synaptobrevin complexes (*9*, *40*).

connection between syntaxin conformation and self-association, we conducted additional proteolysis experiments at a protein concentration favoring self-association (40 μM) and at a protein concentration where both syntaxin constructs are primarily monomeric (0.1 μM). For both syntaxin 1−253 and syntaxin 1−265, the site of initial proteolytic cleavage was found to vary with protein concentration, providing direct evidence that self-association is influencing protein conformation in this system. In each case, high concentrations (left panels in Figure 5) promoted cleavage between residues 179 and 180, resulting in the early accumulation of fragment C. For example, whereas the initial cleavage of syntaxin 1−253 at lower concentrations strongly favors fragment B, at high concentrations B and C appear with a similar time course. Conversely, at low concentrations (right panels in Figure 5), initial cleavage for both proteins is at the site between residues 220 and 221, and fragment B is produced preferentially. Furthermore, the accelerated disappearance of syntaxin 1−265 compared to that of syntaxin 1−253 is not seen at this low concentration, confirming that the relatively greater protease sensitivity of syntaxin 1−265 is caused by self-association. Thus, two lines of evidence from proteolysis experiments indicate that conformational changes accompany self-association: at each protein concentration, syntaxin 1−253 and syntaxin 1−265 display different protease sensitivity, and for each protein construct, protease sensitivity varies with protein concentration.

DISCUSSION

The structure of an N-terminal domain of syntaxin-1A was determined at 1.9 Å resolution by MAD phasing. The structure comprises a three-helix bundle with a conserved hydrophobic groove. This groove in the N-terminal domain likely interacts with juxtamembrane residues nearer the C-terminus of the intact protein to create a "closed" conformation. Further evidence for this closed protein conformation comes from proteolytic data: significant accumulation of syntaxin 1−220 (B in Figure 5) is seen in all protease protection experiments conducted under "monomer" conditions (0.1 and 2 μM for syntaxin 1−253, and 0.1 μM for syntaxin 1−265). This fragment corresponds to a hypothetical closed conformation including the N-terminal domain and a large portion of the juxtamembrane region (Figure 6). This work therefore adds to previous evidence suggesting that syntaxin can adopt a closed conformation that might regulate its interactions with other proteins (*7*, *11*−*13*, *16*).

Previous experiments had suggested that the histidine-tagged cytoplasmic domain of syntaxin is monomeric at relatively high salt concentrations (300 mM) (*6*), while intact syntaxin (including the transmembrane domain) forms SDS-stable dimers (*33*). Here, we use equilibrium analytical ultracentrifugation over a broad range of protein concentrations to demonstrate that even the cytoplasmic domain of untagged syntaxin self-associates under conditions that approximate physiological ionic strength.

Formation of dimers or larger homomultimers has also been observed for other t-SNAREs and may be biologically significant. The cytoplasmic domains of yeast SNAREs, including Sed5 (L. Cavanaugh and F. M. Hughson, unpublished results) and Pep12 (*34*), have been observed to dimerize in vitro. In addition, *Drosophila* Sed5 dimers are formed in transfected COS cell membranes, as judged by chemical cross-linking, and this dimerization requires the

juxtamembrane domain (*35*). Most models for SNARE function have suggested that the hetero-oligomerization of v- and t-SNAREs on different membranes plays a central role in the docking and fusion of vesicles with organelles or the plasma membrane (*36*, *37*). Nonetheless, several observations have suggested that t-SNAREs alone can suffice, presumably by forming homomeric complexes that link membranes. For example, homotypic vacuole fusion is only about 2-fold less efficient in vitro when both partners carry only t-SNAREs than it is when one partner carries only v-SNAREs and the other carries only t-SNAREs (*38*). Similarly, the t-SNARE Ufe1 has been shown to oligomerize in vitro and has been proposed to mediate homotypic fusion among endoplasmic reticulum membranes via t-SNARE−t-SNARE interactions (*39*). Though no role for syntaxin oligomers in neurotransmitter release has yet been documented, our results represent the most quantitative analysis to date of t-SNARE self-association. Furthermore, the growing evidence for t-SNARE homo-oligomerization points toward an additional level of promiscuity in SNARE partnering that may be subject to regulatory control in vivo.

Sytaxin undergoes a conformational change upon self-association (Figure 6). The proteolytic sensitivity of the cleavage site between residues 179 and 180 appears to serve as a readout for this change. Strikingly, the same site becomes sensitive when heteromeric SNARE complexes are formed (*9*). Thus, self-association seems to be accompanied by a conformational opening of the closed syntaxin monomers.

Guided by our analysis of protease sensitivitiy as well as the known structural features of heteromeric SNARE complexes, we propose a model for open syntaxin dimers (Figure 6). It seems plausible that the juxtamembrane heptad repeats assemble to form parallel bundles in syntaxin multimers, as seen in heteromeric complexes. Syntaxin 180−265 is protease-resistant under conditions where syntaxin is primarily self-associated (Figure 5), and very similar syntaxin fragments are protease-resistant in heteromeric complexes (*3*, *9*, *40*). Association between transmembrane domains, not present in our study, would further stabilize the parallel helical bundles in homomeric SNARE complexes (see ref *33*). Peptides as short as 32 residues derived from the juxtamembrane region of syntaxin display significant α-helix content by CD at concentrations of 30−60 μM (*41*), presumably due to multimeric associations such as those proposed here. Flexibly attached N-terminal domains, as observed for heteromeric complexes (*1*, *12*), would account for the increased proteolytic susceptibility of the bond between residues 179 and 180. While this model is consistent with the available data, an alternative self-association model involving domain swapping (see ref *42* for review) cannot be ruled out at present. Nonetheless, the parallel bundle model seems more consistent with what is known about heteromeric SNARE complexes, with the protection against further proteolysis of residues 180−265, and with the dimer-destabilizing effect of deleting residues 254−265.

Are there structural constraints that argue against the formation of t-SNARE complexes in which the helical bundle resembles that of heteromeric SNARE complexes? In the only published SNARE complex structure (*3*), four approximately 85-residue protein fragments derived from syntaxin (residues 180−262), SNAP-25, and syntaptobrevin form an elongated bundle of parallel α-helices with a generally hydrophobic core. The bundle contains a single "layer" of polar core residues that serve to determine the register of the four helices (*3*, *8*). Synaptobrevin contributes an Arg residue to this layer, the guanidino group of which is buried within the core of the four-helix bundle. This buried positive charge is neutralized by partial negative charges carried on the side chain oxygens of glutamine side chains contributed by each of the other three helices (*3*). It has been suggested that most SNARE complexes would contain one arginine-containing SNARE and three glutamine-containing SNAREs (*43*). In this model, homomeric SNARE complexes containing four glutamine-containing SNAREs would be disallowed. However, all-glutamine layers are not uncommon in coiled coil cores (unpublished observations), presumably because the partial positive and partial negative characters of each glutamine side chain can compensate one another cyclically around the bundle. Thus, parallel helical bundles with two or more syntaxin molecules are not implausible on first principles.

The stoichiometry of syntaxin−SNAP-25 complexes in vitro is 2:1 (*31*). Therefore, it might be anticipated that syntaxin dimers would be on the kinetic pathway to syntaxin−SNAP-25 complexes. Furthermore, conformational opening of the yeast syntaxin Sso1 accelerates SNARE complex assembly 2000-fold (*12*), further suggesting that the open syntaxin dimers might form complexes with SNAP-25 more readily than the closed monomers. Nonetheless, the rate of assembly with SNAP-25 is only subtly influenced by the conformational opening mediated by syntaxin dimerization (F. M. Hughson, unpublished results). Therefore, contrary to expectation, it appears that the rate-limiting step for assembly in vitro is not strongly sensitive to the oligomeric state of syntaxin. It will be worthwhile in future work to examine whether 1:1 and 2:1 syntaxin−SNAP-25 complexes bind the v-SNARE syntaptobrevin with equal efficiency, or whether the need to displace a syntaxin molecule from the 2:1 complexes slows the formation of the ternary core complex.

Many intracellular trafficking steps appear to require a member of the Sec1 protein family (see ref *44* and references therein). Sec1 family members interact with syntaxin homologues and/or ternary SNARE complexes (*7*, *16*, *44*, *45*), but their molecular roles in vesicle targeting and fusion have been controversial. In vitro, nSec1 binds to a closed form of syntaxin and prevents it from forming heteromeric SNARE complexes (*7*, *15*, *16*, *45*). Our experiments suggest strongly that the closed conformation prevents syntaxin multimerization. Thus, an important function of nSec1 binding may be to block the formation of homomeric syntaxin complexes. nSec1 is well-suited to this role since it binds directly to the juxtamembrane region of syntaxin that mediates multimerization and since it holds syntaxin in a closed conformation incompatible with multimer formation. nSec1 may even serve to chaperone the assembly of the proper SNARE complexes.

ACKNOWLEDGMENT

We thank Larisa Sereda for early contributions to this project, Vibha Rao and the staff of the National Synchrotron Light Source beamline X12C for advice and assistance in X-ray data collection, Saw Kyin for DNA sequencing and

protein microchemistry, Jim Lear for curve fitting procedures, Phyllis Hanson for reagents, and Bill Weis for sharing a manuscript prior to publication. We gratefully acknowledge helpful input from Yigong Shi, Gerry Waters, Jannette Carey, Jeff Gerst, Phyllis Hanson, Graham Warren, and members of the Hughson laboratory.

REFERENCES

1. Hanson, P. I., Roth, R., Morisaki, H., Jahn, R., and Heuser, J. E. (1997) *Cell 90*, 523−535.
2. Weber, T., Zemelman, B. V., McNew, J. A., Westermann, B., Gmachl, M., Parlati, F., Söllner, T. H., and Rothman, J. E. (1998) *Cell 92*, 759−772.
3. Sutton, R. B., Fasshauer, D., Jahn, R., and Brunger, A. T. (1998) *Nature 395*, 347−353.
4. Jahn, R., and Südhof, T. C. (1999) *Annu. Rev. Biochem. 68*, 863−911.
5. Bennett, M. K., Calakos, N., and Scheller, R. H. (1992) *Science 257*, 255−259.
6. Fasshauer, D., Otto, H., Eliason, W. K., Jahn, R., and Brünger, A. T. (1997) *J. Biol. Chem. 272*, 28036−28041.
7. Dulubova, I., Sugita, S., Hill, S., Hosaka, M., Fernandez, I., Sudhof, T. C., and Rizo, J. (1999) *EMBO J. 18*, 4372−4382.
8. Weimbs, T., Low, S. H., Chapin, S. J., Mostov, K. E., Bucher, P., and Hofmann, K. (1997) *Proc. Natl. Acad. Sci. U.S.A. 94*, 3046−3051.
9. Fasshauer, D., Eliason, W. K., Brunger, A. T., and Jahn, R. (1998) *Biochemistry 37*, 10354−10362.
10. Fasshauer, D., Antonin, W., Margittai, M., Pabst, S., and Jahn, R. (1999) *J. Biol. Chem. 274*, 15440−15446.
11. Calakos, N., Bennett, M. K., Peterson, K. E., and Scheller, R. H. (1994) *Science 263*, 1146−1149.
12. Nicholson, K. L., Munson, M., Miller, R. B., Filip, T. J., Fairman, R., and Hughson, F. M. (1998) *Nat. Struct. Biol. 5*, 793−802.
13. Fiebig, K. M., Rice, L. M., Pollock, E., and Brunger, A. T. (1999) *Nat. Struct. Biol. 6*, 117−123.
14. Betz, A., Okamoto, M., Benseler, F., and Brose, N. (1997) *J. Biol. Chem. 272*, 2520−2526.
15. Pevsner, J., Hsu, S.-C., Braun, J. E. A., Calakos, N., Ting, A. E., Bennett, M. K., and Scheller, R. H. (1994) *Neuron 13*, 353−361.
16. Yang, B., Steegmaier, M., Gonzalez, L. C., and Scheller, R. H. (2000) *J. Cell Biol. 148*, 247−252.
17. Fernandez, I., Ubach, J., Dulubova, I., Zhang, X., Südhof, T. C., and Rizo, J. (1998) *Cell 94*, 841−849.
18. Yang, B., Gonzalez, L., Prekeris, R., Steegmaier, M., Advani, R. J., and Scheller, R. H. (1999) *J. Biol. Chem. 274*, 5649−5653.
19. Tsui, M. M., and Banfield, D. K. (2000) *J. Cell Sci. 113*, 145−152.
20. MacFerrin, K. D., Chen, L., Terranova, M. P., Schreiber, S. L., and Verdine, G. L. (1993) *Methods Enzymol. 217*, 79−102.
21. Leahy, D. J., Erickson, H. P., Aukhil, I., Joshi, P., and Hendrickson, W. A. (1994) *Proteins 19*, 48−54.
22. Thogersen, H. C., and Nagai, K. (1987) *Methods Enzymol. 153*, 461−481.
23. Otwinowski, Z., and Minor, W. (1998) *Methods Enzymol. 276*, 307−326.
24. Collaborative Computational Project Number 4 (1994) *Acta Crystallogr. D50*, 760−763.
25. Brünger, A. T. (1992) *X-PLOR (Version 3.1): A System for X-ray Crystallography and NMR*, Yale University Press, New Haven, CT.
26. Brunger, A. T., Adams, P. D., Clore, G. M., Delano, W. L., Gros, P., Grosse-Kunstleve, R. W., Jiang, J.-S., Kuszewski, J., Nilges, N., Pannu, N. S., Read, R. J., Rice, L. M., Simonson, T., and Warren, G. L. (1998) *Acta Crystallogr. D54*, 905−921.
27. Jones, T. A., Zou, J.-Y., Cowan, S. W., and Kjeldgaard, M. (1991) *Acta Crystallogr. A47*, 110−119.
28. Laue, T. M., Shah, B. D., Ridgeway, T. M., and Pelletier, S. L. (1992) in *Analytical Ultracentrifugation in Biochemistry and Polymer Science* (Harding, S. E., Rowe, A. J., and Horton, J. C., Eds.) pp 90−125, The Royal Society of Chemistry, Cambridge, U.K.
29. Tjandra, N., and Bax, A. (1997) *Science 278*, 1111−1114.
30. Schiavo, G., Shone, C. C., Bennett, M. K., Scheller, R. H., and Montecucco, C. (1995) *J. Biol. Chem. 270*, 10566−10570.
31. Fasshauer, D., Bruns, D., Shen, B., Jahn, R., and Brünger, A. T. (1997) *J. Biol. Chem. 272*, 4582−4590.
32. Rice, L. M., Brennwald, P., and Brünger, A. T. (1997) *FEBS Lett. 415*, 49−55.
33. Margittai, M., Otto, H., and Jahn, R. (1999) *FEBS Lett. 446*, 40−44.
34. Tishgarten, T., Yin, F. F., Faucher, K. M., Dluhy, R. A., Grant, T. R., Fischer von Mollard, G., Stevens, T. H., and Lipscomb, L. A. (1999) *Protein Sci. 8*, 2465−2473.
35. Banfield, D. K., Lewis, M. J., Rabouille, C., Warren, G., and Pelham, H. R. B. (1994) *J. Cell Biol. 127*, 357−371.
36. Hughson, F. M. (1999) *Curr. Biol. 9*, R49−R52.
37. Mayer, A. (1999) *Curr. Opin. Cell Biol. 11*, 447−452.
38. Nichols, B. J., Ungermann, C., Pelham, H. R. B., Wickner, W. T., and Haas, A. (1997) *Nature 387*, 199−202.
39. Patel, S. K., Indig, F. E., Olivieri, N., Levine, N. D., and Latterich, M. (1998) *Cell 92*, 611−620.
40. Poirer, M. A., Hao, J. C., Malkus, P. N., Chan, C., Moore, M. F., King, D. S., and Bennett, M. K. (1998) *J. Biol. Chem. 273*, 11370−11377.
41. Zhong, P., Chen, Y. A., Tam, D., Chung, D., Scheller, R. H., and Miljanich, G. P. (1997) *Biochemistry 36*, 4317−4326.
42. Schlunegger, M. P., Bennett, M. J., and Eisenberg, D. (1997) *Adv. Protein Chem. 50*, 61−122.
43. Fasshauer, D., Sutton, R. B., Brunger, A. T., and Jahn, R. (1998) *Proc. Natl. Acad. Sci. U.S.A. 95*, 15781−15786.
44. Carr, C. M., Grote, E., Munson, M., Hughson, F. M., and Novick, P. J. (1999) *J. Cell Biol. 146*, 333−344.
45. Misura, K. M. S., Scheller, R. H., and Weis, W. I. (2000) *Nature 404*, 355−362.
46. Esnouf, R. M. (1997) *J. Mol. Graphics Modell. 15*, 132−134.
47. Kraulis, P. (1991) *J. Appl. Crystallogr. 24*, 924−950.
48. Merritt, E. A., and Bacon, D. J. (1997) *Methods Enzymol. 277*, 505−524.
49. Nicholls, A., Sharp, K. A., and Honig, B. (1991) *Proteins 11*, 281−296.
50. Johnson, M. L., Correia, J. J., Yphantis, D. A., and Halverson, H. R. (1981) *Biophys. J. 36*, 575−588.

BI0003994